

1 Individualized multi-omic pathway deviation scores

2 using multiple factor analysis

3 Andrea Rau^{1,2}, Regina Manansala², Michael J. Flister³,

4 Hallgeir Rui³, Florence Jaffrézic¹, Denis Laloë^{1*}, Paul L. Auer^{2*}

5
6 ¹ GABI, INRA, AgroParisTech, Université Paris-Saclay, 78350, Jouy-en-Josas, France

7 ² Joseph J. Zilber School of Public Health, University of Wisconsin-Milwaukee, Milwaukee, WI 53201, USA

8 ³ Department of Pathology, Medical College of Wisconsin, Milwaukee, WI 53226, USA

9 * Corresponding authors: denis.laloe@inra.fr, pauer@uwm.edu

10 11 **ABSTRACT**

12
13 Malignant progression of normal tissue is typically driven by complex networks of somatic
14 changes, including genetic mutations, copy number aberrations, epigenetic changes, and
15 transcriptional reprogramming. To delineate aberrant multi-omic tumor features that correlate with
16 clinical outcomes, we present a novel pathway-centric tool based on the multiple factor analysis
17 framework called *padma*. Using a multi-omic consensus representation, *padma* quantifies and
18 characterizes individualized pathway-specific multi-omic deviations and their underlying drivers,
19 with respect to the sampled population. We demonstrate the utility of *padma* to correlate patient
20 outcomes with complex genetic, epigenetic, and transcriptomic perturbations in clinically
21 actionable pathways in breast and lung cancer.

22
23 **Keywords:** Multi-omic data, multiple factor analysis, pathways, cancer genomics

27 BACKGROUND

28

29 Large sets of patient-matched multi-omics data have become widely available for large-scale
30 human health studies in recent years, with notable examples including the [The Cancer Genome](#)
31 [Atlas](#) (TCGA)¹ and Trans-omics for Precision Medicine ([TOPMed](#)) program. The increasing
32 emergence of multi-omic data has in turn led to a renewed interest in multivariate, multi-table
33 approaches² to account for interdependencies within and across data types³. In such large-scale
34 multi-level data, there is often limited or incomplete *a priori* knowledge of relevant phenotype
35 groups for comparisons, and a primary goal may be to identify subsets of individuals that share
36 common molecular characteristics, design therapies in the context of personalized medicine, or
37 identify relevant biological pathways for follow-up. With these goals in mind, many multivariate
38 approaches have the advantage of being unsupervised, using matched or partially matched omics
39 data across genes, obviating the need for predefined groups for comparison as in the framework
40 of standard differential analyses. A variety of such approaches has been proposed in recent
41 years. For example, Multi-omics Factor Analysis (MOFA) uses group factor analysis to infer sets
42 of hidden factors that capture biological and technical variability for downstream use in sample
43 clustering, data imputation, and sample outlier detection⁴.

44

45 In multi-omic integrative analyses, an intuitive first approach is to consider a gene-centric analysis,
46 as we previously proposed in the *EDGE in TCGA* tool⁵. Expanding such analyses to the pathway-
47 level is also of great interest, as it can lead to improved biological interpretability as well as
48 reduced or condensed gene lists to facilitate the generation of relevant hypotheses. In particular,
49 our goal is to define a method that quantifies an individual's deviation from a sample average, at
50 the pathway-level, while simultaneously accounting for multiple layers of molecular information.
51 Several related approaches for pathway-specific single-sample analyses have been proposed in
52 recent years⁶⁻⁸. For example, PARADIGM⁷ is a widely used approach based on structured

53 probabilistic factor graphs to prioritize relevant pathways involved in cancer progression as well
54 as identify patient-specific alterations; both pathway structures and multi-omic relationships are
55 hard-coded directly in the model, but it requires a discretization of the data and is now a closed-
56 source software, making extensions and application to other gene sets difficult. Pathway
57 relevance ranking⁹ integrates binarized tumor-related omics data into a comprehensive network
58 representation of genes, patient samples, and prior knowledge to calculate the relevance of a
59 given pathway to a set of individuals. A pathway-centric supervised principal component-based
60 analysis implemented in *pathwayPCA*¹⁰ performs gene selection and estimates latent variables
61 for association testing with respect to binary, continuous, and survival outcomes within each set
62 of omics data independently. Pathifier⁶ instead seeks to calculate a personal pathway
63 deregulation score (PDS), based on the distance of a single individual from the median reference
64 sample on a principal curve; this principal curve approach is analogous to a nonlinear principal
65 components analysis (PCA), but can be applied only to a single-omic dataset (e.g., gene
66 expression). For both PARADIGM and Pathifier, clusters of scores across pathways are shown
67 to correlate with clinically relevant clustering of patients.

68
69 Here, we extend the basic philosophy of the Pathifier approach to multi-omics data, using an
70 innovative application of a Multiple Factor Analysis (MFA), to quantify individualized pathway
71 deviation scores. In particular, we propose an approach called *padma* (“Pathway Deviation scores
72 using Multiple factor Analysis”) to characterize individuals with aberrant multi-omic profiles for a
73 given pathway of interest and to quantify this deviation with respect to the sampled population
74 using a multi-omic consensus representation. We further investigate the following succession of
75 questions. In which pathways are high deviation scores strongly associated with measures of
76 poor prognosis? For such pathways, which specific individuals are characterized by the most
77 highly aberrant multi-omic profile? And for such individuals, which specific genes and omics drive
78 large pathway deviation scores? By providing graphical and numerical outputs to address these

79 questions, *padma* represents both an approach for generating hypotheses as well as an
80 exploratory data analysis tool for identifying individuals and genes/omics of potential interest for
81 a given pathway.

82

83 There is already some precedent for using MFA to integrate multi-omic data, although existing
84 approaches differ from that proposed here. For instance, de Tayrac et al. suggested using MFA
85 for paired CGH array and microarray data, superimposed with functional gene ontology terms, to
86 highlight common structures and provide graphical outputs to better understand the relationships
87 between omics¹¹. In addition, *padma* shares some similarities with a recently proposed integrative
88 multi-omics unsupervised gene set analysis called *mogsa*, which is similarly based on a MFA¹².
89 By calculating an integrated multi-omics enrichment score for a given gene set with respect to the
90 full gene list, *mogsa* identifies gene sets driven by features that explain a large proportion of the
91 global correlated information among different omics. In addition, these integrated enrichment
92 scores can be decomposed by omic and used to identify differentially expressed gene sets or
93 reveal biological pathways with correlated profiles across multiple complex data sets. However,
94 the fundamental difference in the two approaches is that *mogsa* evaluates pathway-specific
95 enrichment with respect to the entire set of genes, while *padma* instead focuses on identifying
96 and quantifying pathway-specific multi-omic deviations between each individual and the sampled
97 population.

98

99 **RESULTS AND DISCUSSION**

100

101 **Description of the approach**

102

103 *Pathway-centric multiple factor analysis for multi-omic data*

104

105 MFA represents an extension of principal component analysis for the case where multiple
106 quantitative data tables are to be simultaneously analyzed^{13–16}. As such, MFA is a dimension
107 reduction method that decomposes the set of features from a given gene set into a lower
108 dimension space. In particular, the MFA approach weights each table individually to ensure that
109 tables with more features or those on a different scale do not dominate the analysis; all features
110 within a given table are given the same weight. These weights are chosen such that the first
111 eigenvalue of a PCA performed on each weighted table is equal to 1, ensuring that all tables play
112 an equal role in the global multi-table analysis. According to the desired focus of the analysis,
113 data can be structured either with molecular assays (e.g., RNA-seq, methylation, miRNA-seq,
114 copy number alterations) as tables (and genes as features within omics), or with genes as tables
115 (and molecular assays as features within genes). The MFA weights balance the contributions of
116 each omic or of each gene, respectively. In this work, we focus on the latter strategy in order to
117 allow different omics to contribute to a varying degree depending on the chosen pathway. In
118 addition, we note that because the MFA is performed on standardized features, simple differences
119 in scale between omics (e.g., RNA-seq log-normalized counts versus methylation logit-
120 transformed beta values) do not impact the analysis.

121
122 More precisely, consider a pathway or gene set composed of p genes (Figure 1A), each of which
123 is measured using up to k molecular assays (e.g., RNA-seq, methylation, miRNA-seq, copy
124 number alterations), contained in the set of gene-specific matrices X_1, \dots, X_p that have the same
125 n matched individuals (rows) and j_1, \dots, j_p potentially unmatched variables (columns) in each,
126 where $j_g \in \{1, \dots, k\}$ for each gene $g = 1, \dots, p$. Because only the observations and not the
127 variables are matched across data tables, genes may be represented by potentially different
128 subset of omics data (e.g., only expression data for one gene, and expression and methylation
129 data for another).

130

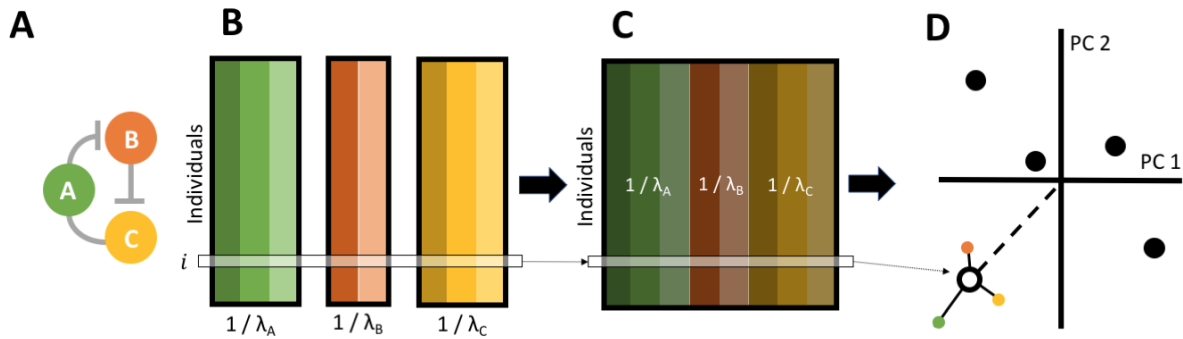
131 In the first step, these data tables are generally standardized (i.e., centered and scaled). Next, an
132 individual PCA is performed using singular value decomposition for each gene table X_g , and its
133 largest singular value λ_g^1 is calculated (Figure 1B). Then, all features in each gene table X_g are
134 weighted by $\frac{1}{\lambda_g^1}$, and a global PCA is performed using a singular value decomposition on the
135 concatenated set of weighted standardized tables, $X^* = \left[\frac{X_1}{\lambda_1^1}, \dots, \frac{X_p}{\lambda_p^1} \right]$ (Figure 1C). This yields a
136 matrix of components (i.e., latent variables) in the observation and variable space. Optionally, an
137 independent set of supplementary individuals (or supplementary variables) can then be projected
138 onto the original representation; this is performed by centering and scaling variables for the
139 supplementary individuals (or individuals for the supplementary variables, respectively) to the
140 same scale as for the reference individuals, and projecting these rescaled variables into the
141 reference PCA space. Note that in the related *mogsa* approach, supplementary binary variables
142 representing gene membership in gene sets are projected onto a transcriptome-wide multiple
143 factor analysis to calculate gene set scores¹².

144

145 The MFA thus provides a consensus across-gene representation of the individuals for a given
146 pathway, and the global PCA performed on the weighted gene tables decomposes the consensus
147 variance into orthogonal variables (i.e., principal components) that are ordered by the proportion
148 of variance explained by each. The coordinates of each individual on these components, also
149 referred to as factor scores, can be used to produce factor maps to represent individuals in this
150 consensus space such that smaller distances reflect greater similarities among individuals. In
151 addition, *partial factor scores*, which represent the position of individuals in the consensus for a
152 given gene, can also be represented in the consensus factor map; the average of partial factor
153 scores across all dimensions and genes for a given individual corresponds to the factor score

154 (Figure 1D). A more thorough discussion of the MFA, as well as its relationship to a PCA, may be
155 found in the Supplementary Methods.

156



157

158 **Figure 1.** Illustration of the *padma* approach for calculating individualized multi-omic
159 pathway deviation scores. (A-B) For a given pathway, matched multi-omic measures for
160 each gene are assembled, with individuals in rows. Note that genes may be assayed for
161 varying types of data (e.g., measurements for one gene may be available for expression,
162 methylation, and copy number alterations, while another may only have measurements
163 available for expression and methylation). (C) Using a Multiple Factor Analysis, each gene
164 table is weighted by its *largest singular value*, and per-gene weighted tables are combined
165 into a global table, which in turn is analyzed using a Principal Component Analysis. (D)
166 Finally, each individual *i* is projected onto the consensus pathway representation; the
167 individualized pathway deviation score is then quantified as the distance of this individual
168 from the average individual. These scores can be further decomposed into parts attributed
169 to each gene in the pathway.

170

171 *Individualized pathway deviation scores*

172

173 In the consensus space obtained from the MFA, the origin represents the “average” pathway
174 behavior across genes, omics, and individuals; individuals that are projected to increasingly

175 distant points in the factor map represent those with increasingly aberrant values, with respect to
176 this average, for one or more of the omics measures for one or more genes in the pathway. To
177 quantify these aberrant individuals, we propose an individualized pathway deviation score d_i
178 based on the multidimensional Euclidean distance of the MFA component loadings for each
179 individual to the origin:

$$180 \quad d_i^2 = \sum_{l=1}^L f_{i,l}^2,$$

181 where $f_{i,l}$ corresponds to the MFA factor score of individual i in component l , and L corresponds
182 to the rank of X^* . Note that this corresponds to the weighted Euclidean distance of the scaled
183 multi-omic data (for the genes in a given pathway) of each individual to the origin. These
184 individualized pathway deviation scores are thus nonnegative, where smaller values represent
185 individuals for whom the average multi-omic pathway variation is close to the average, while larger
186 scores represent individuals with increasingly aberrant multi-omic pathway variation with respect
187 to the average. An individual with a large pathway deviation score is thus characterized by one or
188 more genes, with one or more omic measures, that explain a large proportion of the global
189 correlated information across the full pathway.

190
191 Note that the full set of components is used for this deviation calculation, rather than subsetting
192 to an optimal number of components; we remark that due to their small variance relative to lower
193 dimensions, components from larger dimensions contribute relatively little to the overall pathway
194 deviation scores. Finally, to facilitate comparisons of scores calculated for pathways of differing
195 sizes (e.g., the number of genes), deviation scores with respect to the origin are normalized for
196 the pathway size.

197 *Decomposition of individualized pathway deviation scores into per-gene contributions*

198

199 In order to quantify the role played by each gene for each individual, we decomposed the
200 individualized pathway deviation scores into gene-level contributions. Recall that the average of
201 partial factor scores across all MFA dimensions corresponds to each individual's factor score. We
202 define the gene-level deviation for a given individual as follows:

$$203 \quad d_{i,g} = \frac{\sum_{l=1}^L f_{i,l}(f_{i,l,g} - f_i)}{\sum_{l=1}^L f_{i,l}^2},$$

204 where as before $f_{i,l}$ corresponds to the MFA factor score of individual i in component l , L
205 corresponds to the rank of X^* , and $f_{i,l,g}$ corresponds to the MFA partial factor score of individual i
206 in gene g in component l . Note that by construction, the contributions of all pathway genes to the
207 overall deviation score sum to 0. In particular, per-gene contributions can take on both negative
208 and positive values according to the extent to which the gene influences the deviation of the
209 overall pathway score from the origin (i.e., the global center of gravity across individuals); large
210 positive values correspond to genes with a large influence on the overall deviation of an individual,
211 while large negative values correspond to genes that tend to be most similar to the global average.
212 In the following, we additionally scale these per-gene scores by the inverse overall pathway score
213 to highlight genes with highly atypical multi-omic measures both with respect to other genes in
214 the pathway and with respect to individuals in the population.

215

216 *Quantifying percent contribution of omics to pathway-centric multiple factor analysis*

217

218 The richness of MFA outputs also includes various decompositions of the total variance (that is,
219 the sum of the variances of each individual MFA component) of the multi-omic data for a given
220 pathway. Similarly to a standard PCA, the percent contribution of each axis of the MFA can be
221 calculated as the ratio between the variance of the corresponding MFA component and the total
222 variance; by construction, the fraction of explained variance explained decreases as the MFA

223 dimension increases. Similarly, the percent contribution to the inertia of each axis for a given omic,
224 gene, or individual can be quantified as the ratio between the inertia of its respective partial
225 projection in the consensus space and the inertia of the full data projection for that axis. These
226 per-gene, per-omic, and per-individual contributions can be quantified for a subset of components
227 (e.g., the first ten dimensions) or for the entire set of components; here, as we calculate
228 individualized pathway deviation scores using the full set of dimensions, we also calculated a
229 weighted per-omic contribution, which corresponds to the average contribution across all
230 dimensions, weighted by the corresponding eigenvalue.

231

232 **Application**

233

234 *TCGA data acquisition and pre-processing*

235

236 We illustrate the utility of *padma* on data from two cancer types with sufficiently large multi-omic
237 sample sizes in the TCGA database: invasive breast carcinoma (BRCA), which was chosen as
238 individuals have previously been classified into one of five molecular subtypes¹⁷ (Luminal A,
239 Luminal B, Her2+, Basal, and Normal-like), as well as lung adenocarcinoma (LUAD), which was
240 chosen for its high recorded mortality.

241

242 The *padma* approach integrates multi-omic data by mapping omics measures to genes in a given
243 pathway. Although this assignment of values to genes is straightforward for RNA-seq, CNA, and
244 methylation data, a definitive mapping of miRNA-to-gene relationships does not exist, as miRNAs
245 can each potentially target multiple genes. Many methods and databases based on text-mining
246 or bioinformatics-driven approaches exist to predict miRNA-target pairs¹⁸. Here, we make use of
247 the curated miR-target interaction (MTI) predictions in miRTarBase (version 7.0)¹⁹, using only

248 exact matches for miRNA IDs and target gene symbols and predictions with the “Functional MTI”
249 support type. Although the TCGA data used here have been filtered to include only those genes
250 for which expression measurements are available, there are cases where missing values are
251 recorded in other omics datasets (e.g., when no methylation probe was available in the promoter
252 region of a gene, or when no predicted MTIs were identified) or where a given feature has little or
253 no variance across individuals. In this analysis, features for a given omics dataset were removed
254 from the analysis only if missing values are recorded for all individuals or if the feature has minimal
255 variance across all individuals (defined here as $< 10^{-5}$ after scaling). After running *padma*, we
256 remark that the first ten MFA dimensions represent a large proportion of the total multi-omic
257 variance across pathways for both cancers (Supplementary Figure 5; BRCA median = 46.1%,
258 LUAD median = 51.9%).

259
260 As a measure of patient prognosis, we focused on two different metrics. First, we used the
261 standardized and curated clinical data included in the TCGA Pan-Cancer Clinical Resource
262 (TCGA-CDR)²⁰ to identify the progression-free interval (PFI). The PFI corresponds to the period
263 from the date of diagnosis until the date of the first occurrence of a new tumor event (e.g.,
264 locoregional recurrence, distant metastasis) and typically has a shorter minimum follow-up time
265 than measures such as overall survival. In the BRCA data, a total of 72 uncensored and 434
266 censored events were recorded (median PFI time of 792 and 915 days, respectively); among
267 LUAD individuals, a total of 65 uncensored and 79 censored events were recorded (median PFI
268 time of 439 and 683 days, respectively). Second, we used the histological grade for breast cancer,
269 which is an established cancer hallmark of cellular de-differentiation and poor prognosis²¹
270 (downloaded from http://legacy.dx.ai/tcga_breast on March 7, 2019). Tumors are typically graded
271 by pathologists on a scale of 1 (well-differentiated), 2 (moderately differentiated), or 3 (poorly
272 differentiated) based on three different measures, including nuclear pleomorphism,

273 glandular/tubule formation, and mitotic index, where higher grades correspond to faster-growing
274 cancers that are more likely to spread (Supplementary Table 1).

275

276 *Large deviation scores for relevant oncogenic pathways are associated with survival in lung*
277 *cancer*

278

279 The first question we address is the prioritization of pathways that are associated with a given
280 phenotype of interest. After processing the TCGA data and assembling the collection of gene
281 sets, we sought to identify a subset of pathways for which deviation scores were significantly
282 associated with patient outcome, as measured by PFI. To focus on pathways with the largest
283 potential signal (i.e., those for which a small number of individuals have very large deviation
284 scores relative to the remaining individuals) we consider only those with the most highly positively
285 skewed distribution of deviation scores. For each of the top 5% of pathways ($n = 57$) ranked
286 according to their Pearson's moment coefficient of skewness, we fit a Cox proportional hazards
287 (PH) model for the PFI on the pathway deviation score. Using the Benjamini-Hochberg²² adjusted
288 p-values from a likelihood ratio test (FDR < 5%), we identified 14 pathways with deviation scores
289 that were significantly associated with the progression-free interval in lung cancer (Table 1; see
290 Supplementary Table 2 for the full gene lists in each pathway); for all of these, higher pathway
291 scores corresponded to a worse survival outcome. Note that the filtering on skewness of the
292 pathway scores is performed completely independently of the survival phenotype, ensuring that
293 the downstream survival analysis is not biased²³. Of note, while candidates within the majority
294 deviated pathways (Table 1) have been univariately associated with patient outcome (e.g., cell
295 cycle, DNA repair, and apoptosis^{24,25}), the *padma* TCGA analysis is unique in its ability to extend
296 these associations across multiple gene patient-specific perturbations within a pathway at the
297 genomic and transcriptomic RNA levels.

298

299 The detection of several pathways related to DNA repair (ATM, Homologous DNA repair,
300 BRCA1/2-ATR; Table1), as well as cell cycle and apoptosis related pathways, prompted us to
301 consider is whether these pathway deviation scores are simply acting as proxies for the tumor
302 mutational burden (i.e., the total number of nonsynonymous mutations) for each individual. To
303 investigate this, we estimated the mutational burden for each individual by counting the number
304 of somatic nonsynonymous mutations in a set of cancer-specific driver genes ($n=183$ and $n=181$
305 genes in breast and lung cancer, respectively) identified by IntOGen²⁶. After adding a constant of
306 1 to these counts and log-transforming them, we fit a linear model to evaluate their association
307 with the pathway deviation scores; after correcting p-values from the Wald test statistic for multiple
308 testing (FDR < 10%), no pathways were found to be associated with the mutational burden. In
309 addition, when repeating the Cox PH model described above including the log-mutational burden
310 as an additional covariate, adjusted p-values were generally similar to previous values, and the
311 top six pathways remained significant at a significance threshold of 5%. This suggests that the
312 biological signal contained in the pathway deviation scores is indeed independent of that linked
313 to mutational burden.
314

Pathway name	Pathway database	Adj. p-value	Hazard ratio	# of genes
D4-GDI (GDP dissociation inhibitor) signaling pathway	Biocarta	0.0111	1.2692	13
NF-kB activation through FADD/RIP-1 pathway mediated by caspase-8 and -10	Reactome	0.0111	1.2839	12
Class I PI3K signaling events mediated by Akt	PID	0.0251	1.1700	35
ATM signaling pathway	Biocarta	0.0265	1.1644	20
CARM1 and regulation of the estrogen receptor	Biocarta	0.0265	1.1426	35
Homologous recombination repair of replication-independent double-strand breaks	Reactome	0.0265	1.2432	16
Role of BRCA1, BRCA2, and ATR in cancer susceptibility	Biocarta	0.0467	1.1823	21

CD40L signaling pathway	Biocarta	0.0467	1.1880	15
Induction of apoptosis through DR4 and DR4/5 death receptors	Biocarta	0.0467	1.1208	33
Cell cycle: G1/S check point	Biocarta	0.0467	1.1263	28
Double stranded RNA induced gene expression	Biocarta	0.0467	1.2007	10
Signaling events mediated by HDAC class III	PID	0.0467	1.1543	25
HIV-1 Nef: Negative effector of Fas and TNF-alpha	PID	0.0467	1.1268	35
Regulation of telomerase	PID	0.0467	1.0950	68

315 **Table 1.** Pathways whose deviation scores are significantly correlated with progression-
316 free interval in lung cancer. Hazard ratios and adjusted p-values correspond to a Cox PH
317 model for pathway deviation alone, with FDR < 5%. The number of genes for each pathway
318 corresponds to the number of genes with expression quantified by RNA-seq in the TCGA
319 data.

320

321 *Padma identifies individualized aberrations in the D4-GDP dissociation inhibitor signaling*
322 *pathway in lung cancer*

323

324 To illustrate the full range of results provided by *padma*, we focus in particular on the results for
325 the *D4-GDP dissociation inhibitor (GDI) signaling* pathway. D4-GDI is a negative regulator of the
326 ras-related Rho Family of GTPases, and it has been suggested that it may promote breast cancer
327 cell proliferation and invasiveness^{27,28}. The D4-GDI signaling pathway is made up of 13 genes;
328 RNA-seq, methylation, and CNA measures are available for all 13 genes, with the exception of
329 CYCS and PARP1, for which no methylation probes were measured the promoter region. In
330 addition, miRNA-seq data were included for one predicted target pair: hsa-mir-421 → CASP3.
331 Over the 13 genes in the pathway, 130 of the 144 individuals had no nonsynonymous mutations,
332 while 13 and 1 individuals had 1 or 3 such mutations; ARHGAP5 and CASP3 were most often
333 characterized by mutations (3 individuals affected for each). Notably, although the D4-GDI

334 pathway has been previously implicated in breast cancer aggressiveness^{27,28}, this is to our
335 knowledge the first evidence suggesting that D4-GDI pathway might play a similar role in
336 promoting lung cancer.

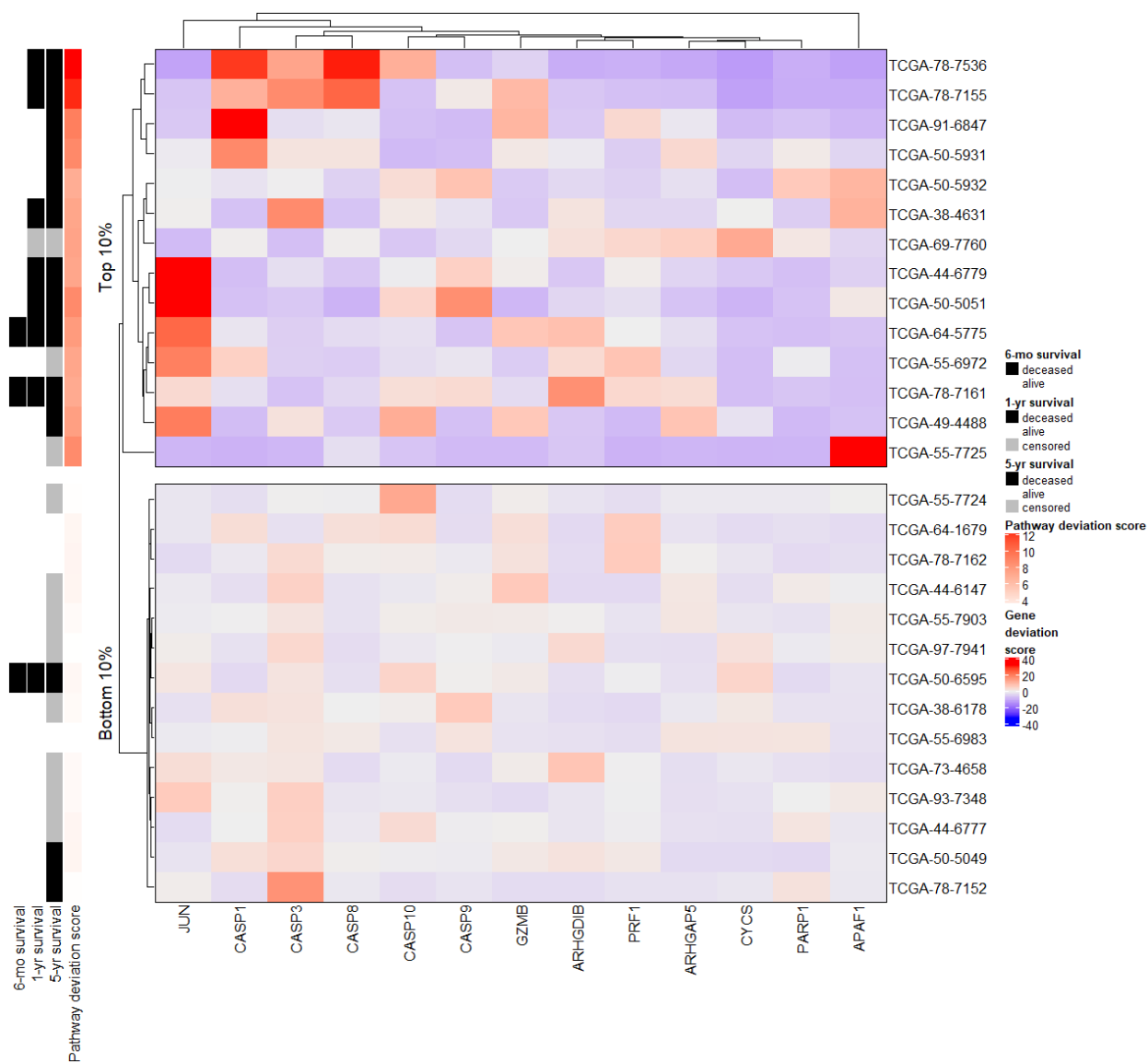
337

338 Using the multi-omic data available for the D4-GDI signaling pathway, we can use the outputs of
339 *padma* to better understand the individualized drivers of multi-omic variation. In particular, it is
340 possible to quantify both gene-specific deviation scores as well as an overall pathway deviation
341 score for each individual, respectively based on the set of partial or full MFA components. We first
342 visualize the scaled gene-specific deviation scores for the top and bottom decile of individuals,
343 according to their overall pathway deviation score (Figure 2); these groups thus correspond to the
344 individuals that are least and most similar to the average individual within the population. We
345 remark that the 10% of individuals with the most aberrant overall scores for the D4-GDI signaling
346 pathway, who also had a high 1- and 5-year mortality rate, are those that also tend to have large
347 aberrant (i.e., red in the heatmap) scaled gene-specific deviation scores for one or more genes.
348 For example, the two individuals with the largest overall scores, TCGA-78-7536 and TCGA-78-
349 7155 (12.79 and 12.31, respectively), both had large scaled gene-specific scores for CASP3
350 (12.93 and 17.05, respectively), CASP1 (27.80 and 10.85, respectively), and CASP8 (29.72 and
351 22.61, respectively). While a subset of five individuals from the top decile were all characterized
352 by high deviation scores for JUN (TCGA-64-5775, TCGA-55-6972, TCGA-50-5051, TCGA-44-
353 6779, TCGA-49-4488), several other genes appear to have relatively small deviation scores for
354 all individuals plotted here (e.g., PRF1, PARP1). In addition, we remark the presence of highly
355 individualized gene-specific aberrations (e.g., APAF1 in individual TCGA-55-7725).

356

357 To provide an intuitive link between these gene-specific deviation scores with the original batch-
358 corrected multi-omics data that were input into *padma*, we further focus on the three genes
359 (CASP1, CASP3, and CASP8) for which large deviation scores were observed for the two highly

360 aberrant individuals (TCGA-78-7536 and TCGA-78-7155) in the D4-GDI signaling pathway. We
361 plot boxplots of the Z-scores for each available omic for the three genes across all 144 individuals
362 with lung cancer (Figure 3), specifically highlighting the two aforementioned individuals; full plots
363 of all 13 genes in the pathway are included in Supplementary Figure 1. This plot reveals that both
364 individuals are indeed notable for their overexpression, with respect to the other individuals, of
365 miRNA hsa-mir-421 (Figure 3D), which is predicted to target CASP3; in coherence with this, both
366 individuals had weaker CASP3 expression than average (although we note that its expression
367 was not particularly extreme with respect to the full sample). Individual TCGA-78-7536 appears
368 to have a hypomethylated CASP1 promoter, but a significantly higher number of copies of CASP8,
369 while individual TCGA-78-7155 is characterized by a large underexpression of CASP8 with
370 respect to other individuals. Both individuals appear to have deletions of CASP3, and
371 hypermethylated CASP8 promoters. This seems to indicate that, although the large overall
372 pathway deviations for these two individuals share some common etiologies, each also exhibit
373 unique characteristics.
374



375

376

377

378

379

380

381

382

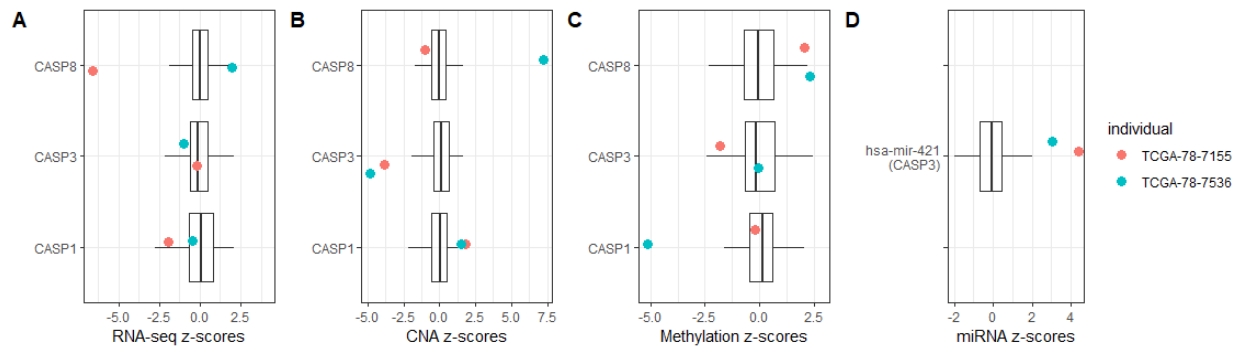
383

384

Figure 2. Scaled per-gene deviation scores for the D4-GDI signaling pathway for individuals corresponding to the top and bottom decile of overall pathway deviation scores. Red scores correspond to highly aberrant gene scores with respect to each individual's global score, while blue indicates gene scores close to the overall population average. Annotations on the left indicate the 6-month, 1-year, and 5-year survival status (deceased, alive, or censored) and overall pathway deviation score for each individual. Genes and individuals within each sub-plot are hierarchically clustered using the Euclidean distance and complete linkage.

385

386



387

388

389 **Figure 3.** Boxplots of Z-scores of gene expression (A), copy number alterations (B),
390 methylation (C), and miRNA expression (D) for all individuals with lung cancer, with the 3
391 genes (CASP1, CASP3, CASP8) and one miRNA (hsa-mir-421, predicted to target
392 CASP3) of interest in the D4-GDI signaling pathway. The two individuals with the largest
393 pathway deviation score (TCGA-78-7155, TCGA-78-7536) are highlighted in red and
394 turquoise, respectively.

395

396

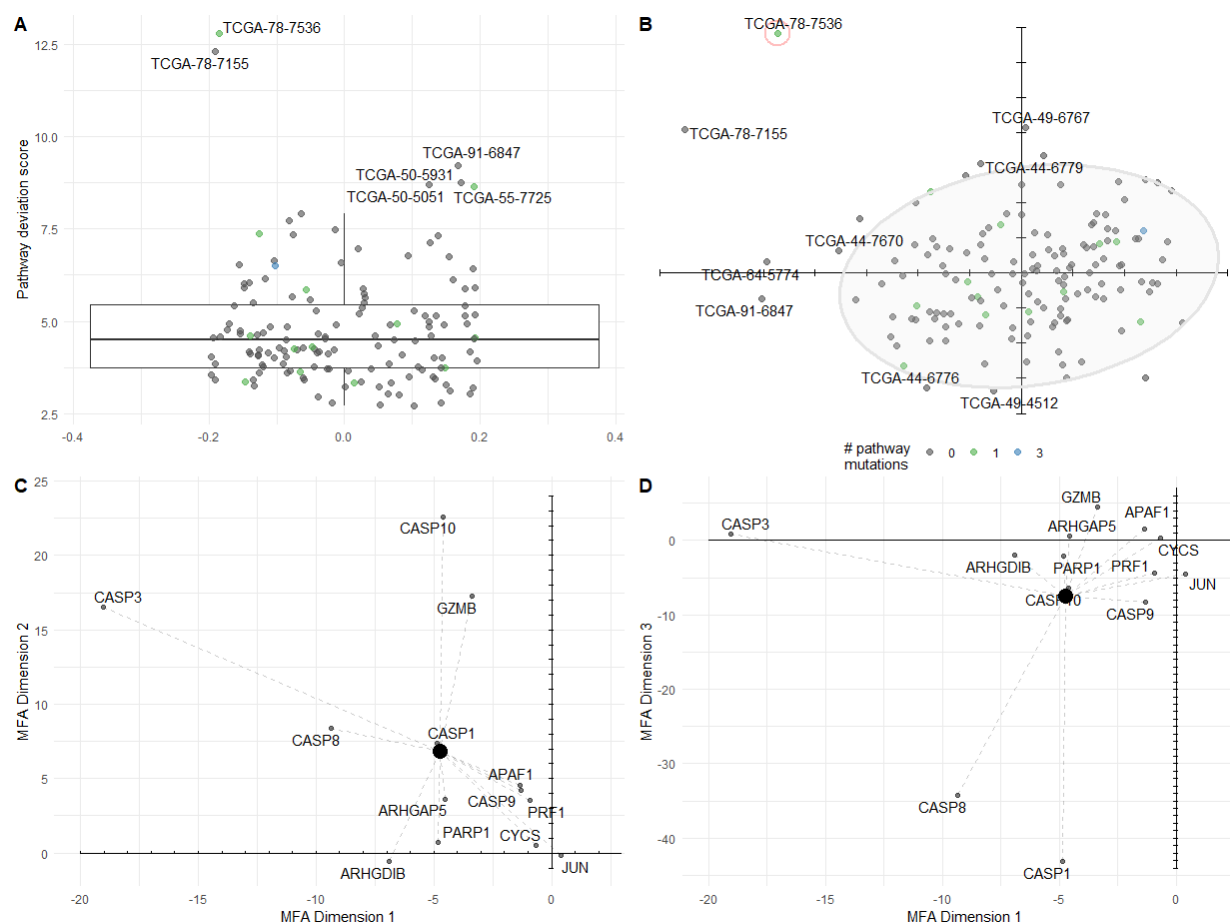
397 As overall pathway deviation scores represent the multi-dimensional average of these gene-
398 specific deviation scores, a deeper investigation into them can also provide useful insight for a
399 given pathway. We first note that the distribution of deviation scores for the D4-GDI signaling
400 pathway (Figure 4A) is highly skewed, with a handful of individuals (e.g., TCGA-78-7536, TCGA-
401 78-7155, TCGA-91-6847, TCGA-50-5931, TCGA-50-5051, and TCGA-66-7725) characterized by
402 particularly large scores with respect to the remaining individuals. The individual with the most
403 aberrant score for this pathway, TCGA-78-7536, had a single pathway-specific somatic mutation
404 in the CASP1 gene, and a total of 7 cancer-specific driver gene mutations (corresponding to the
405 80th percentile of individuals considered here). Although these pathway deviation scores are
406 calculated across all dimensions of the MFA, it can also be useful to represent individuals in the

407 first few components of the consensus MFA space (Figure 4B); the farther away an individual is
408 from the origin over multiple MFA dimensions, the larger the corresponding pathway deviation
409 score. In this case, we see that TCGA-78-7536 is a large positive and negative outlier in the
410 second (9.55% total variance explained), and third (8.07% total variance explained) MFA
411 components, respectively, although less so in the first component (11.97% total variance
412 explained). In addition, we note that RNA-seq is the major driver of the first MFA dimension
413 (54.38% contribution), while promoter methylation and copy number alterations take a larger role
414 in the second and third dimensions (42.29% and 59.18% contribution, respectively). miRNA
415 expression appears to play a fairly minor role in the MFA, with its maximum contribution (21.14%)
416 occurring at only the 16th dimension.

417

418 When examining the partial factor maps for this individual over the first three MFA dimensions
419 (Figures 4C-D), we note the large contribution of CASP3 (axis 1), CASP10 (axis 2), CASP1 and
420 CASP 8 (axis 3), as evidenced by their distance from the origin in these dimensions. Overall, this
421 is coherent with the previous gene-level analyses (Figure 2), where hypomethylation in CASP1
422 and large copy number gains for CASP3 and CASP8 with respect to the population were identified
423 for this individual. Other individuals with large overall deviation scores (e.g., TCGA-50-5931) are
424 not obvious outliers in the first two MFA dimensions, reflecting the fact that additional dimensions
425 play a more important role for them. Taken together, the individualized gene-specific and overall
426 pathway deviation scores output by *padma* provide complementary and interesting exploratory
427 insight into atypical multi-omic profiles for a given pathway of interest (here, the D4-GDI signaling
428 pathway in lung cancer).

429



430

431

432

433

434

435

436

437

438

439

440

441

442

Figure 4. (A) Distribution of pathway deviation scores for the D4-GDI signaling pathway in lung cancer; individuals with unusually large scores are labeled. (B) Factor map, representing the first two components of the MFA for the D4-GDI signaling pathway in lung cancer, with normal confidence ellipse superimposed. Individuals with extreme values in each plot are labeled with their barcode identifiers and colored by the number of pathway-specific nonsynonymous mutations. For the individual circled in red, TCGA-78-7536, a partial factor map representing the first MFA components 1 and 2 is plotted in (C), and MFA components 1 and 3 in (D). The large black dot represents the individual's overall pathway deviation score, as plotted in panel (B) for the first two axes, and gene-specific scores are joined to this point with dotted lines.

443 *Pathway deviation scores globally recapitulate histological grade in breast cancer*

444

445 For some cancers, additional clinical phenotypes beyond survival information may be of particular
446 interest; to illustrate the use of *padma* in such a case, we focus on histological grade for breast
447 cancer. To quantify whether pathway deviation scores tend to be associated with histological
448 grade in breast cancer, we performed a one-way ANOVA on the three measures that comprise
449 histological grade for each of the 1136 pathways. Based on the Benjamini-Hochberg²² adjusted
450 p-values from an F-test (FDR < 5%), all (1136) or nearly all (1135) pathways were found to have
451 deviation scores that are significantly correlated with mitotic index and nuclear pleomorphism.
452 Intriguingly, no pathways were found to be associated with degree of glandular/tubule formation;
453 this may in part be due to the large proportion of individuals identified as grade III (poorly
454 differentiated) for this measure ($n = 285$). The rankings of pathways based on mitotic index and
455 nuclear pleomorphism were generally in agreement (Supplementary Figure 2). In all but two
456 cases, higher deviation pathway scores corresponded to the higher grades for these two
457 measures, corresponding to more aggressive tumors; the two exceptions were the *Presynaptic*
458 *nicotinic acetylcholine receptor* and *Highly calcium permeable postsynaptic nicotinic acetylcholine*
459 *receptor* pathways (both from Reactome), for which the largest pathway deviation scores were
460 associated with grade II, rather than grade III, of the mitotic index.

461

462 To prioritize pathways among this list, we calculated the rank product of the individual rankings
463 by *p*-value for mitosis and nuclear pleomorphism; the top 10 pathways according to this joint
464 ranking are shown in Table 2 (see Supplementary Table 3 for the full gene lists in each pathway).
465 The *signaling by Wnt* pathway, which is made up of 63 genes, had the highest combined ranking
466 for these two histological measures. Of this set of genes, all had RNA-seq, methylation, and CNA
467 measures available, with the exception of FAM123B and PSMD10 (no CNA measures with
468 nonzero variance) and PSMB1 to PSMB10, PSMC2, PSMC3, PSMC5, PSMC6, PSME1, and

469 PSME2 (no promoter methylation measures). miRNA-seq data were included for only two
 470 predicted target pairs: hsa-mir-375 →CTNNB1 and hsa-mir-320a →CTNNB1. Over the 63 genes
 471 in the pathway, 453 individuals had no nonsynonymous mutations, while 39, 6, 3, 2, and 1
 472 individuals had 1, 2, 3, 4, or 5 such mutations; APC, PSMD1, and FAM123B were most often
 473 characterized by mutations (10, 7, and 7 individuals affected, respectively).
 474

Pathway name	Pathway database	Combined ranking	# of genes
Signaling by Wnt	Reactome	3.16	63
Apoptotic execution phase	Reactome	5.00	52
APC/C:Cdh1 mediated degradation of Cdc20 and other APC/C:Cdh1 targeted proteins in late mitosis/early G1	Reactome	6.78	64
Genes involved in Beta-catenin phosphorylation cascade	Reactome	10.49	16
Autodegradation of Cdh1 by Cdh1:APC/C	Reactome	10.95	56
Genes involved in M/G1 transition	Reactome	11.62	72
Regulation of the Fanconi anemia pathway	Reactome	13.93	7
Apoptotic cleavage of cellular proteins	Reactome	14.14	38
Apoptosis	Reactome	14.28	143
ER-phagosome pathway	Reactome	15.62	58

475 **Table 2.** Pathways whose deviation scores are significantly correlated with measures of
 476 histological grade (mitosis, nuclear pleomorphism) in breast cancer. Adjusted p-values
 477 after Benjamini-Hochberg correction were $< 3.31 \times 10^{-12}$ for all pathways presented in the
 478 table. Combined ranks correspond to the rank product of the individual rankings from
 479 mitosis and nuclear pleomorphism, and the number of genes for each pathway
 480 corresponds to the number of genes with expression quantified by RNA-seq in the TCGA
 481 data.

482
 483 Similarly to the distribution of D4-GDI pathway scores in lung adenocarcinomas, a small number
 484 of breast cancer patients are characterized by highly aberrant scores in the signaling by Wnt

485 pathway, including TCGA-BH-A1FM, TCGA-E9-A22G, and TCGA-EW-A1PH, and the number of
486 pathway-specific nonsynonymous somatic mutations does not appear to be related to this score.
487 The associated factor map on the first two dimensions of the MFA (Figure 5A) clearly captures
488 relevant biological structure from the data, as evidenced by the quasi-separation of individuals in
489 different intrinsic inferred molecular subtypes (AIMS). Notably, individuals with Basal and Luminal
490 A breast cancer are clearly separated in the first two dimensions and tend to respectively have
491 positive and negative loadings in the first dimension of the MFA; Luminal B and Normal-like
492 subtypes largely overlap with the Luminal A subtype for this pathway, while Her2 is located
493 intermediate to the Luminal and Basal subtypes, as could be anticipated due to the equal
494 prevalence of Her2 amplification in both Luminal and Basal subtypes. Similar relevant biological
495 signal can be seen when considering a larger spectrum of pathways (Figure 5C). In particular,
496 individuals with the Basal and Luminal B subtypes tend to have much more highly variant
497 deviation scores across all pathways, whereas Luminal A and Normal-like subtypes are generally
498 much less variant.

499

500 When examining the percent contribution of each omic to the axes of the MFA for the Wnt
501 signaling pathway (Figure 5B), we remark the preponderant contribution of gene expression to
502 the first component (84.40%), while variability in the second component is largely driven by both
503 gene expression and copy numbers (45.66 and 35.37%, respectively). The large role played by
504 RNA-seq here is coherent with the definition of the AIMS subtypes themselves, which are defined
505 on the basis of gene expression. On average, after weighting by the eigenvalue of each
506 component, gene expression and copy number alterations were found to have similar
507 contributions to the overall variation (36.6%, 35.4%, respectively), while methylation played a less
508 important role (26.8%). For this pathway, as for most others we studied (Supplementary Figure
509 6), miRNA expression contributed relatively little to the overall variation (1.2%).

510

511 Taken together, these results illustrate that the *padma* approach, which is used in an
512 unsupervised manner on multi-omic cancer data for a given pathway, is able to recapitulate known
513 sample structure in the form of intrinsic tumor subtypes as well as relevant prognostic factors such
514 as histological grade.

515

516 **CONCLUSIONS**

517

518 Unsupervised dimension reduction approaches (such as PCA) have been widely used in genetics
519 and genomics for many years, both to identify sample structure and batch effects²⁹ and to
520 visualize overall variation in large data³⁰. Here, we present a generalization of this approach to
521 multi-omic data for investigating biological variation at the pathway-level by aggregating across
522 genes, omic-type, and individuals. Compared to single-omics approaches (for instance, running
523 a PCA on RNA-seq data alone), *padma* accommodates multiple omics-sources which, for some
524 sample sets and pathways, account for more than 50% of the overall variation (Figure 5B). Using
525 MFA to partition variance, we construct a clinically relevant pathway disruption score that
526 correlates with survival outcomes in lung cancer patients, and histological grade in breast cancer
527 patients.

528

529 Our MFA-based approach allows investigators to (a) identify overall sources of variation (such as
530 batch effects); (b) prioritize high variance pathways defined by variability across subjects; (c)
531 identify aberrant observations (i.e., individuals) within a given pathway; and (d) identify the genes
532 and omics sources that drive these aberrant observations. For large, multi-omic data such as
533 TCGA, *padma* allows investigators to summarize overall variation and assist in generating
534 hypotheses for more targeted analyses and follow-up studies. As a case in point, we identified
535 two lung cancer patients with aberrant multi-omic profiles at three *CASP* genes. With access to

536 the tumor samples and more fine-grained clinical data, future molecular experiments could help
537 to clarify the role (if any) that these genes play in contributing to lung cancer mortality.

538

539 There are a number of natural extensions and alternative formulations to our MFA-based
540 approach. If comparisons between sets of individuals (e.g., healthy vs. disease) are of interest,
541 the MFA can be based on one set of samples (e.g., healthy, or a “reference set”), and the other
542 set of samples (e.g., diseased, or a “supplementary set”) can be projected onto this original
543 representation. This is accomplished by centering and scaling supplementary individuals to the
544 same scale as the reference individuals, and projecting these rescaled variables into the
545 reference MFA space. In this setting, the interpretation of pathway deviation scores would no
546 longer correspond to the identification of “aberrant” individuals compared to an overall average,
547 but rather individuals that are most different from the reference set (e.g., the most “diseased” as
548 compared to a healthy reference); this strategy would be similar in spirit to the individualized
549 pathway aberrance score (iPAS) approach, which proposed using accumulated (unmatched)
550 normal samples as a reference set³¹. There is also no reason to limit this approach to pathways,
551 as the analysis could be performed just once, genome-wide (accordingly, inferences would no
552 longer be applicable to specific pathways). Here, we have structured the data with genes
553 representing data tables and omics representing columns within each table. Alternatively, the
554 data could be re-weighted by having omics represented as data tables and genes as columns
555 within each, similar to de Tayrac et al. (2009)¹¹. Extensions to our work could include incorporating
556 the hierarchical structure of genes within pathways, or relatedness structure among samples. In
557 principle, other types of omics that do not map to genes or pathways (e.g., genotypes on single
558 nucleotide polymorphisms) could also be incorporated. Finally, though we illustrate the use of
559 *padma* for cancer genomics data, we anticipate that it will be broadly useful to other multi-omic
560 applications in human health or agriculture.

561

562 MATERIALS AND METHODS

563

564 *TCGA data acquisition and pre-processing*

565

566 The multi-omic TCGA data were downloaded and processed as described in Rau et al. (2019)⁵.
567 Briefly, using *TCGA2STAT*³² we downloaded processed TCGA Level 3 data from the Broad
568 Institute Genome Data Analysis Center (GDAC) Firehose on March 18, 2017 for individuals of
569 self-reported European ancestry for whom gene expression, methylation, copy number alterations
570 (CNA), microRNA (miRNA) abundance, and somatic mutation data were all available; this
571 ancestry filter was applied to minimize population-specific variance and focus on the group with
572 the largest available sample size. In addition, two individuals from the BRCA dataset (TCGA-E9-
573 A245, TCGA-BH-A1ES) were identified as outliers with consistently extreme deviation scores
574 across multiple pathways and were removed from the remainder of the analyses; the final sample
575 sizes were thus $n=504$ and $n=144$ individuals for the BRCA and LUAD datasets, respectively.

576

577 Per-gene normalized expression estimates were calculated using RSEM³³. Methylation was
578 quantified using the maximally variant probe from the Illumina Infinium Human Methylation450
579 BeadChip located within ± 1500 bp of the transcription start site, and representative probe beta
580 measures were transformed to the logit scale. Somatic CNAs were called by comparing Affymetrix
581 6.0 probe intensities from normal (i.e., non-cancer tissue) and cancer tissue, and genome
582 segments were aggregated to gene-level measures by *TCGA2STAT* and *CNTools*. Individuals
583 were classified as carriers or noncarriers of a nonsynonymous somatic mutation for each gene
584 using *TCGA2STAT*. Normalized miRNA abundance was quantified as Reads per million
585 microRNA mapped (RPMMM) values. RNA-seq and miRNA-seq quantifications were TMM-
586 normalized³⁴, converted to counts per million (CPM), and log₂-transformed. Only genes with
587 available RNA-seq expression measures were retained for the remainder of the analysis,

588 corresponding to 20,501 and 19,971 genes for BRCA and LUAD, respectively. Finally, batch
589 effects have been shown to have a strong impact on the analysis of high-throughput data in
590 general²⁹ and for the TCGA data specifically³⁵. As specific sample plates have been shown to
591 represent significant batch effects in previous analyses³⁶, each processed omic (with the
592 exception of somatic mutation data) was individually batch adjusted for each cancer to correct for
593 plate-specific effects using `removeBatchEffects` in `limmal`³⁷. Plots of the first two components
594 from a transcriptome-wide and genome-wide single-omics PCA and multi-omics MFA for the
595 batch-corrected data are included in Supplementary Figures 3 and 4.

596

597 *Choice of curated pathway collection*

598

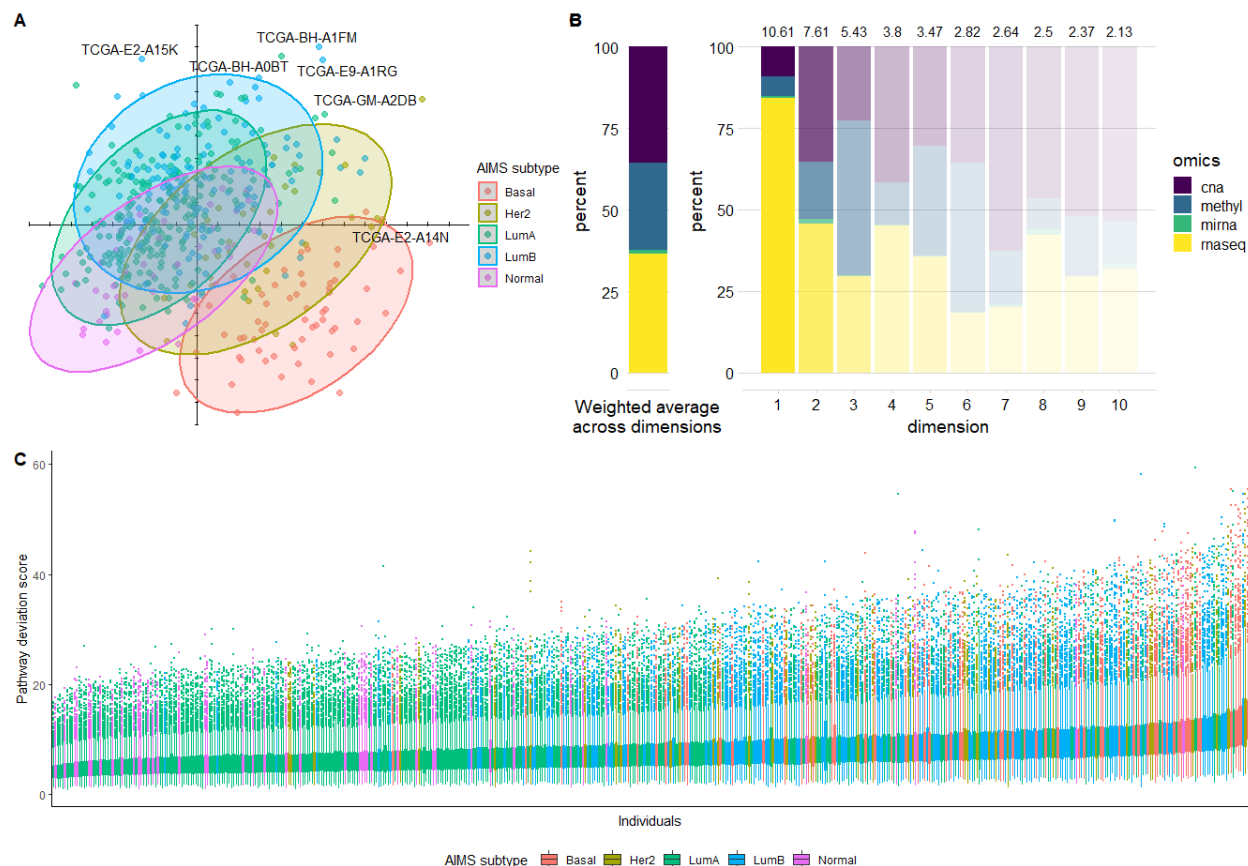
599 We consider the pathways included in the MSigDB [canonical pathways](#) curated gene set
600 catalog³⁸, which includes genes whose products are involved in metabolic and signaling pathways
601 reported in curated public databases. We specifically use the “C2 curated gene sets” catalog from
602 MSigDB v5.2 available at <http://bioinf.wehi.edu.au/software/MSigDB/> as described in the *limma*
603 Bioconductor package³⁷. We focus in particular on a collection of 1322 gene sets from public
604 databases, including Biocarta, Pathway Interaction Database³⁹, Reactome⁴⁰; [Sigma Aldrich](#),
605 [Signaling Gateway](#), [Signal Transduction Knowledge Environment](#), and the Matrisome Project⁴¹,
606 the smallest and largest of which were respectively made up of 6 and 478 genes (median size 29
607 genes). For the subsequent *padma* analysis, we excluded gene sets for which fewer than 3 genes
608 mapped to quantified features in the TCGA gene expression data, corresponding to a total of
609 1136 gene sets.

610

611 *Padma R software package*

612 The proposed method described above has been implemented in an open-source R package
 613 called *padma*, freely available on [GitHub](#). *Padma* notably makes use *FactoMineR*^{3,15} to run the
 614 MFA; heatmaps in the following results were produced using *ComplexHeatmap*⁴². All of the
 615 analyses in this paper were performed using R v3.5.1.

616



617
 618 **Figure 5.** (A) Factor map of individuals, representing the first two components of the MFA,
 619 for the Wnt signaling pathway in breast cancer, with normal confidence ellipses
 620 superimposed for the five AIMS subtypes. B) Weighted overall percent contribution per
 621 omic (left) and for each of the first 10 MFA components (right) for the Wnt signaling
 622 pathway, with colors faded according to the percent variance explained for each
 623 (represented in text above each bar). (C) Distribution of pathway deviation scores for each
 624 individual in the breast cancer data, with individuals colored according to their AIMS
 625 subtype.

626

627 **DECLARATIONS**

628

629 *Ethics approval and consent to participate:* Not applicable.

630 *Consent for publication:* Not applicable.

631 *Availability of data and materials:* The TCGA data analysed in the current study were retrieved
632 and pre-processed as described in the Methods section and in Rau et al. (2018)⁵; in particular, all
633 associated scripts can be found at <https://github.com/andreamrau/EDGE-in-TCGA>
634 (<https://doi.org/10.5281/zenodo.3524080>). All R scripts used to generate the results in this work
635 may be found at https://github.com/andreamrau/RMFRJLA_2019, and the associated *padma* R
636 package may be found at <https://github.com/andreamrau/padma>.

637 *Competing interests:* The authors declare that they have no competing interests.

638 *Funding:* Dr. Andrea Rau was supported by the AgreeSkills+ fellowship program, which received
639 funding from the EU's Seventh Framework Program under grant agreement FP7-60939
640 (AgreeSkills+ contract).

641 *Authors' contributions:* AR conceived and designed the study, wrote the *padma* R package,
642 analyzed the data, and drafted the manuscript. RM analyzed the data and contributed to the R
643 package development. MJF and HR interpreted results and contributed to study design. FJ
644 contributed to the study conception and writing of the manuscript. DL supervised the study
645 conception and method implementation and drafted the manuscript and supplementary materials.
646 PLA conceived and designed the study and drafted the manuscript. All authors read and approved
647 the final manuscript.

648 *Acknowledgements:* Not applicable.

649 REFERENCES

650

651 1. The Cancer Genome Atlas Research Network *et al.* The Cancer Genome Atlas Pan-Cancer
652 analysis project. *Nat. Genet.* **45**, 1113–1120 (2013).

653 2. Meng, C. *et al.* Dimension reduction techniques for the integrative analysis of multi-omics
654 data. *Brief. Bioinform.* **17**, 628–641 (2016).

655 3. Husson, F., Lê, S. & Pagès, J. *Exploratory multivariate analysis by example using R*. (CRC
656 Press, 2017).

657 4. Argelaguet, R. *et al.* Multi- Omics Factor Analysis—a framework for unsupervised integration
658 of multi- omics data sets. *Mol. Syst. Biol.* **14**, (2018).

659 5. Rau, A., Flister, M., Rui, H. & Auer, P. L. Exploring drivers of gene expression in the Cancer
660 Genome Atlas. *Bioinformatics* (2018) doi:10.1093/bioinformatics/bty551.

661 6. Drier, Y., Sheffer, M. & Domany, E. Pathway-based personalized analysis of cancer. *Proc.*
662 *Natl. Acad. Sci.* **110**, 6388–6393 (2013).

663 7. Vaske, C. J. *et al.* Inference of patient-specific pathway activities from multi-dimensional
664 cancer genomics data using PARADIGM. *Bioinformatics* **26**, i237–i245 (2010).

665 9. Verbeke, L. P. C. *et al.* Pathway Relevance Ranking for Tumor Samples through Network-
666 Based Data Integration. *PLOS ONE* **10**, e0133503 (2015).

667 10. Odom, G. J. *et al.* *pathwayPCA: an R package for integrative pathway analysis with*
668 *modern PCA methodology and gene selection*. <http://biorxiv.org/lookup/doi/10.1101/615435>
669 (2019) doi:10.1101/615435.

670 11. de Tayrac, M., Le, S., Aubry, M., Mosser, J. & Husson, F. Simultaneous analysis of
671 distinct Omics data sets with integration of biological knowledge: Multiple Factor Analysis
672 approach. *BMC Genomics* **10**, 32 (2009).

673 12. Meng, C. *et al.* MOGSA: Integrative Single Sample Gene-set Analysis of Multiple Omics

- 674 Data. *Mol. Cell. Proteomics* **18**, S153–S168 (2019).
- 675 13. Escofier, B. & Pagès, J. *Analyses factorielles simples et multiples: objectifs, méthodes et*
676 *interprétation*. (2014).
- 677 14. Pagès, J. *Multiple factor analysis by example using R*. (CRC Press, Taylor & Francis
678 Group, 2015).
- 679 15. Lê, S., Josse, J. & Husson, F. **FactoMineR** : An R Package for Multivariate Analysis. *J.*
680 *Stat. Softw.* **25**, (2008).
- 681 16. Abdi, H., Williams, L. J. & Valentin, D. Multiple factor analysis: principal component
682 analysis for multitable and multiblock data sets: Multiple factor analysis. *Wiley Interdiscip.*
683 *Rev. Comput. Stat.* **5**, 149–179 (2013).
- 684 17. Paquet, E. R. & Hallett, M. T. Absolute assignment of breast cancer intrinsic molecular
685 subtype. *J. Natl. Cancer Inst.* **107**, 357 (2015).
- 686 18. Riffo-Campos, Á., Riquelme, I. & Brebi-Mieville, P. Tools for Sequence-Based miRNA
687 Target Prediction: What to Choose? *Int. J. Mol. Sci.* **17**, 1987 (2016).
- 688 19. Chou, C.-H. *et al.* miRTarBase update 2018: a resource for experimentally validated
689 microRNA-target interactions. *Nucleic Acids Res.* **46**, D296–D302 (2018).
- 690 20. Liu, J. *et al.* An Integrated TCGA Pan-Cancer Clinical Data Resource to Drive High-
691 Quality Survival Outcome Analytics. *Cell* **173**, 400-416.e11 (2018).
- 692 21. Heng, Y. J. *et al.* The molecular basis of breast cancer pathological phenotypes:
693 Molecular basis of breast cancer pathological phenotypes. *J. Pathol.* **241**, 375–391 (2017).
- 694 22. Benjamini, Y. & Hochberg, Y. Controlling the False Discovery Rate: A Practical and
695 Powerful Approach to Multiple Testing. *J. R. Stat. Soc. Ser. B Methodol.* **57**, 289–300 (1995).
- 696 23. Bourgon, R., Gentleman, R. & Huber, W. Independent filtering increases detection
697 power for high-throughput experiments. *Proc. Natl. Acad. Sci.* **107**, 9546–9551 (2010).
- 698 24. Bosken, C. H., Wei, Q., Amos, C. I. & Spitz, M. R. An analysis of DNA repair as a
699 determinant of survival in patients with non-small-cell lung cancer. *J. Natl. Cancer Inst.* **94**,

- 700 1091–1099 (2002).
- 701 25. Singhal, S., Vachani, A., Antin-Ozerkis, D., Kaiser, L. R. & Albelda, S. M. Prognostic
702 implications of cell cycle, apoptosis, and angiogenesis biomarkers in non-small cell lung
703 cancer: a review. *Clin. Cancer Res. Off. J. Am. Assoc. Cancer Res.* **11**, 3974–3986 (2005).
- 704 26. Gonzalez-Perez, A. *et al.* IntOGen-mutations identifies cancer drivers across tumor
705 types. *Nat. Methods* **10**, 1081–1082 (2013).
- 706 27. Zhang, Y., Rivera Rosado, L. A., Moon, S. Y. & Zhang, B. Silencing of D4-GDI inhibits
707 growth and invasive behavior in MDA-MB-231 cells by activation of Rac-dependent p38 and
708 JNK signaling. *J. Biol. Chem.* **284**, 12956–12965 (2009).
- 709 28. Zhang, Y. & Zhang, B. D4-GDI, a Rho GTPase regulator, promotes breast cancer cell
710 invasiveness. *Cancer Res.* **66**, 5592–5598 (2006).
- 711 29. Leek, J. T. *et al.* Tackling the widespread and critical impact of batch effects in high-
712 throughput data. *Nat. Rev. Genet.* **11**, 733–739 (2010).
- 713 30. Novembre, J. *et al.* Genes mirror geography within Europe. *Nature* **456**, 98–101 (2008).
- 714 31. Ahn, T., Lee, E., Huh, N. & Park, T. Personalized identification of altered pathways in
715 cancer using accumulated normal tissue data. *Bioinformatics* **30**, i422–i429 (2014).
- 716 32. Wan, Y.-W., Allen, G. I. & Liu, Z. TCGA2STAT: simple TCGA data access for integrated
717 statistical analysis in R. *Bioinforma. Oxf. Engl.* **32**, 952–954 (2016).
- 718 33. Li, B. & Dewey, C. N. RSEM: accurate transcript quantification from RNA-Seq data with
719 or without a reference genome. *BMC Bioinformatics* **12**, 323 (2011).
- 720 34. Robinson, M. D. & Oshlack, A. A scaling normalization method for differential expression
721 analysis of RNA-seq data. *Genome Biol.* **11**, R25 (2010).
- 722 35. Akulenko, R., Merl, M. & Helms, V. BEclear: Batch Effect Detection and Adjustment in
723 DNA Methylation Data. *PLOS ONE* **11**, e0159921 (2016).
- 724 36. *MBatch: TCGA Batch Effects Viewer.* (2019).
- 725 37. Ritchie, M. E. *et al.* limma powers differential expression analyses for RNA-sequencing

- 726 and microarray studies. *Nucleic Acids Res.* **43**, e47–e47 (2015).
- 727 38. Liberzon, A. *et al.* Molecular signatures database (MSigDB) 3.0. *Bioinformatics* **27**,
- 728 1739–1740 (2011).
- 729 39. Schaefer, C. F. *et al.* PID: the Pathway Interaction Database. *Nucleic Acids Res.* **37**,
- 730 D674–D679 (2009).
- 731 40. Fabregat, A. *et al.* The Reactome Pathway Knowledgebase. *Nucleic Acids Res.* **46**,
- 732 D649–D655 (2018).
- 733 41. Naba, A. *et al.* The Matrisome: *In Silico* Definition and *In Vivo* Characterization by
- 734 Proteomics of Normal and Tumor Extracellular Matrices. *Mol. Cell. Proteomics* **11**,
- 735 M111.014647 (2012).
- 736 42. Gu, Z., Eils, R. & Schlesner, M. Complex heatmaps reveal patterns and correlations in
- 737 multidimensional genomic data. *Bioinformatics* **32**, 2847–2849 (2016).
- 738

739

740 **Supplementary Materials**

741

742 **Supplementary Figure 1.** Z-scores of RNA-seq, CNA, methylation, and miRNA-seq data for
743 genes in the D4-GDI signaling pathway for individuals in the TCGA LUAD data (n = 144). Data
744 corresponding to the two individuals with the largest overall pathway deviation scores, TCGA-78-
745 7155 and TCGA-78-7536, are highlighted in red and blue.

746

747 **Supplementary Figure 2.** Negative log₁₀-transformed p-values from the ANOVA F-test of
748 pathway deviation score versus mitosis and nuclear pleomorphism for each pathway among
749 breast cancer individuals. The signaling by Wnt pathway is highlighted in red.

750

751 **Supplementary Figure 3.** Factor maps for the first two dimensions of a global transcriptome- and
752 genome-wide PCA of the methylation, miRNA-seq, CNA, and RNA-seq data (left), as well as a
753 global MFA of all four omics combined (right) for the TCGA BRCA data.

754

755 **Supplementary Figure 4.** Factor maps for the first two dimensions of a global transcriptome- and
756 genome-wide PCA of the methylation, miRNA-seq, CNA, and RNA-seq data (left), as well as a
757 global MFA of all four omics combined (right) for the TCGA BRCA data.

758

759 **Supplementary Figure 5.** Percent variance explained by the first 5 (blue) or 10 (red) components
760 of the MFA for each pathway for the TCGA BRCA (A) and LUAD (B) data.

761

762 **Supplementary Figure 6.** Average percent contribution to the MFA of each omic (miRNA-seq,
763 methylation, CNA, RNA-seq) for each pathway. (A) Per-omic average contribution across the first

764 10 MFA components for TCGA BRCA. (B) Per-omic average contribution across all MFA
765 components for TCGA BRCA. (C) Per-omic average contribution across the first 10 MFA
766 components for TCGA LUAD. (D) Per-omic average contribution across all MFA components for
767 TCGA LUAD.

768

769 **Supplementary Table 1.** Sample size for each histological measure for the $n = 504$ breast cancer
770 patients.

771

772 **Supplementary Table 2.** Full gene lists for pathways in Table 1. Genes correspond to those with
773 expression quantified by RNA-seq in the TCGA data.

774

775 **Supplementary Table 3.** Full gene lists for pathways in Table 2. Genes correspond to those with
776 expression quantified by RNA-seq in the TCGA data.

777